

U_{re}^0	standard potential of the reference electrode on the absolute thermodynamic scale, V
V	potential difference between metal of the working electrode and the solution just outside the diffuse double layer, V
$V_{o,j}$	value of V when working electrode is at equilibrium in a solution of composition equivalent to that adjacent to the electrode surface
v	bulk fluid velocity, cm/s
y	normal coordinate into the solution from the electrode surface, cm
z_i	charge of species i

Greek

$\alpha_{a,j}$	apparent anodic transfer coefficient for reaction j
$\alpha_{c,j}$	apparent cathodic transfer coefficient for reaction j
β	true transfer coefficient
δ_D	diffusion layer thickness, cm
ρ_0	density of solution, kg/cm ³
Φ	potential in the solution, V
Φ_{met}	potential of working electrode, V
Φ_{re}	potential in the bulk solution at the location of the reference electrode, V
η_j	overpotential of reaction j , V
μ_i	stoichiometric coefficient of species i in a homogeneous reaction
ν	kinematic viscosity, cm ² /s
ξ	dimensionless distance, y/δ_D
Ω	rotation speed, rad/s

Subscripts

o	at the electrode surface
j	reaction, j
re	reference electrode
ref	reference conditions
$bulk$	in the bulk solution

REFERENCES

1. A. J. Appleby and S. Nicholson, *J. Electroanal. Chem.*, **38**, App. 15 (1972).
2. A. J. Appleby and S. Nicholson, *ibid.*, **53**, 105 (1974).
3. A. J. Appleby and S. Nicholson, *ibid.*, **83**, 309 (1977).
4. A. J. Appleby and S. Nicholson, *ibid.*, **112**, 71 (1980).
5. S. W. Smith, W. M. Vogel, and S. Kapelner, *This Journal*, **129**, 1668 (1982).
6. W. M. Vogel, S. W. Smith, and S. Bregoli, *ibid.*, **130**, 574 (1983).
7. B. K. Andersen, Ph.D. Dissertation, Technical University of Denmark, Lyngby, Denmark (1975).
8. C.-Y. Yuh, Ph.D. Thesis, Illinois Institute of Technology, Chicago, IL (1985).
9. J. R. Selman, *Energy*, **16**, 153 (1984).
10. S.-H. Lu, Ph.D. Thesis, Illinois Institute of Technology, Chicago, IL (1985).
11. N. I. Uchida, T. Nishina, Y. Mugikura, and K. Itaya, *J. Electroanal. Chem.*, **206**, 229 (1986).
12. J. Winnick and P. N. Ross, *This Journal*, **128**, 991 (1981).
13. G. Wilemski, *ibid.*, **130**, 117 (1983).
14. H. R. Kunz, L. J. Bregoli, and S. T. Szymanski, *ibid.*, **131**, 2815 (1984).
15. A. Borucka and C. M. Sugiyama, *Electrochim. Acta*, **13**, 1807 (1968).
16. S. H. White and U. M. Twardoch, *ibid.*, **27**, 1599 (1982).
17. P. K. Adanuvor, R. E. White, and S. E. Lorimer, *This Journal*, **134**, 625 (1987).
18. J. S. Newman, "Electrochemical Systems," Prentice-Hall, Inc., Englewood Cliffs, NJ (1973).
19. D. R. Stull and H. Prophet, "The JANAF Tables," 2nd ed., NBS, Washington, DC (1971).
20. N. Godshall, Ph.D. Thesis Stanford University, Stanford, CA (1980).
21. J. Newman, *Ind. Eng. Chem. Fundam.*, **5**, 525 (1966).
22. S. H. White and U. M. Twardoch, in "Molten Carbonate Fuel Cell Technology," (PV 84-13) J. R. Selman and T. D. Claar, Editors, p. 434, The Electrochemical Society Softbound Proceedings Series, Pennington, NJ (1984).
23. H. C. Maru, L. Paetsch, and A. Pigeaud, *ibid.*, p. 20.
24. P. K. Adanuvor and R. E. White, *This Journal*, **135**, 1887 (1988).

Analysis of a Pulsed-Plasma Chemical Vapor Deposition Reactor with Recycle

Sang-Kyu Park* and Demetre J. Economou**

Department of Chemical Engineering, University of Houston, Houston, Texas 77204-4792

ABSTRACT

A simplified model for a time-dependent plasma-assisted chemical vapor deposition reactor was developed based on transport and reaction principles. The model equations were solved by the method of lines using collocation on finite elements for the spatial discretization. Emphasis was placed on the deposition rate and uniformity as a function of reactor operating conditions. A pulsed-plasma reactor was analyzed, and compared to a continuous-wave (CW) plasma reactor. Under conditions which would result in high depletion of the precursor gas in the CW reactor, the pulsed-plasma reactor yielded improved uniformity, albeit the deposition rate was reduced. The effect of a recycle stream on both the CW and pulsed-plasma reactors was also studied. For the CW reactor, recycle was most beneficial under conditions of low depletion of the precursor gas. For cases of intermediate depletion of the precursor gas, a CW reactor with recycle or a combination of pulsed-plasma and recycle can result in nearly uniform deposit without sacrificing the deposition rate. Analytic solutions were derived for the CW reactor with recycle, and for a well-mixed pulsed-plasma reactor. The results apply equally well to pulsed-plasma etching reactors conforming to the model assumptions and operating under corresponding conditions.

Plasma-assisted deposition and etching of thin solid films has emerged as a crucial step in the fabrication of microelectronic components (1), and is expected to become even more important in the future. In plasma processing, a low-pressure gas discharge is used to decompose an otherwise inert gas to produce reactive atoms and radicals. The reactive species interact with a substrate to deposit a thin film or to etch the substrate by forming volatile products (2).

Plasma-assisted chemical vapor deposition (PCVD) is used extensively to grow a variety of thin films including dielectrics (e.g., SiO₂ and Si₃N₄) (3, 4), amorphous hydrogenated silicon a-Si:H (5), polymers (6), and more recently diamond (7). In particular, PCVD is the method of choice when low-temperature deposition is required. For example, PCVD is used to deposit a Si₃N₄ passivation layer over devices in which aluminum metallization prohibits the use of conventional high-temperature CVD methods.

Important goals of PCVD include high deposition rate and uniformity, and high quality of the deposited film.

* Electrochemical Society Student Member.

** Electrochemical Society Active Member.

Owing to the process complexity, selection of plasma reactor operating conditions (such as gas composition and flow rate, pressure, power, and excitation frequency) in an effort to achieve the above goals is currently based on trial-and-error approaches. Mathematical models, in concert with experimental measurements, can assist in the rational design of plasma deposition (and etching) reactors.

One can distinguish two levels of complexity in the plasma deposition process. First, the concentration and energy distribution of electrons, ions, and radicals in the plasma must be determined as a function of reactor operating conditions. Second, the relation between the flux (and energy distribution) of particles bombarding the substrate and the resulting film deposition rate and uniformity, as well as film structure and properties must be established.

Mathematical models of the plasma deposition process have been proposed in order to relate the film deposition rate and uniformity to reactor operating conditions (8-10). These models consider the transport and reaction of the precursor gas and of "radicals" resulting from dissociation of the precursor gas in the plasma. Film growth occurs by diffusion and condensation of the radicals on the deposition surface. The models usually assume simplified kinetics (8-10), although models including detailed kinetics have also appeared (11). All the above models are concerned with continuous-wave (CW) reactor operation in which power at a constant level is continuously delivered to the plasma.

Pulsed-plasma operation is a relatively new approach to PCVD which has been implemented by plasma deposition equipment manufacturers, presumably to improve the film uniformity in channel reactors (12, 13). In this method, the power to the system is modulated (e.g., square-wave modulation) at a frequency much smaller than the usual radio frequencies. However, during the plasma-on period of the modulation, a high frequency (e.g., 13.56 MHz) may be used to achieve more efficient gas dissociation and to avoid charging of dielectric films. Recently, pulsed-plasma operation has been used to influence the film properties and deposition rate (14, 15). For example, superior properties of a-Si:H films and suppression of powder formation were obtained by low frequency (40 Hz) modulation of a RF He/SiH₄ plasma (15). Pulsed-plasma operation has also been used for etching (16), and for the study of plasma reaction kinetics (17). However, despite the interest in pulsed-plasma operation, the authors are not aware of any model to calculate the deposition rate and uniformity in a pulsed-plasma reactor.

Recently we proposed the use of the pulsed-plasma method to improve the uniformity of etching in parallel-plate single wafer reactors (18). In the present work, a simplified mathematical model of a pulsed-plasma CVD reactor was considered. Transport and reaction of a precursor gas and of radicals were included, as was done in previous works on CW reactor models (8-10). Deposition rate and uniformity were examined as a function of reactor operating parameters including the effect of pulse period and duty cycle. The effect of a recycle stream was also examined. The performance of a CW reactor was compared to that of a pulsed-plasma reactor with and without recycle. Furthermore, analytical solutions were derived for the CW reactor with recycle, and for a well-mixed (CSTR) pulsed-plasma reactor.

The following discussion refers mainly to the plasma CVD process. However, the problem formulation may easily be adopted to the plasma etching process. In fact, using similar assumptions, the same equations and boundary conditions apply to both deposition and etching reactors. Therefore, the results of the present study may be used to infer the behavior of a pulsed-plasma etching reactor operating under corresponding conditions.

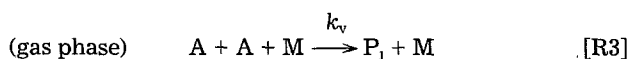
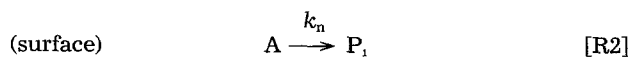
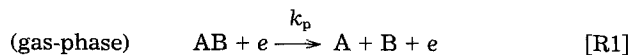
Mathematical Formulation

A schematic of the system studied is shown in Fig. 1. The linear plasma reactor has a constant cross-sectional area along the reactor axis (*x*-axis). Examples include a tubular reactor or a channel reactor formed by two plates separated by a constant spacing. The reactor is equipped with a power supply which can deliver power in a continu-

ous manner or in pulses of varying strength, frequency, and duty cycle. Part of the reactor effluent is recycled and mixed with fresh gas before the mixture enters the reactor. The recycle ratio was defined as

$$R = \frac{\text{volume of effluent gas recycled}}{\text{total volume of effluent gas}} \quad [1]$$

A detailed plasma reactor model must consider the coupled phenomena of potential distribution, transport and reaction of electrons, ions and neutrals, surface reaction kinetics including the effect of ion bombardment, and heat transport in the gas and in the semiconductor wafer. The problem is further complicated by the nonequilibrium nature of the plasma and the large number of species and reactions for which kinetic information is scarce. The present work focuses on the aspect of deposition rate and uniformity along the reactor axis. Therefore, neutral species transport and reaction was emphasized, neglecting the effect of ion bombardment (8-10). The reactions considered are shown schematically below



The precursor gas AB is dissociated in the plasma by electron-impact (reaction [R1]) to produce reactive fragments (radicals) A and B. The radicals are transported about the reactor by diffusion and gas flow and participate in both heterogeneous and homogeneous reactions. In the above reaction scheme, A is assumed to be the main radical containing the depositing species. An important heterogeneous reaction of radical A is deposition (or etching) on a suitable substrate to yield product(s) P_i (reaction [R2]). This reaction may also account for deactivation of the radicals by wall recombination. An important homogeneous (gas-phase) reaction is deactivation by volume recombination, exemplified by reaction [R3]. A third body M is required in order to conserve both momentum and energy during volume recombination. As an example, in the plasma deposition of silicon using silane highly diluted with He, AB = SiH₄, A = SiH_x (x ≤ 3), M = He, and the Si deposit would be one of the products P_j. Of course, the reaction scheme presented above is a simplification of real deposition or etching systems. However, it was felt that the main features of such systems may be captured by using this simplified reaction network (8-10).

In order to further simplify the analysis the following assumptions were introduced:

1. The continuum approximation is valid.
2. The species concentration varies only along the reactor axis, and the flow velocity profile is flat (one-dimensional axial dispersion model).
3. The system is isobaric, isothermal, and isochoric, with constant physical properties.
4. The electron density and energy are spatially uniform and are modulated completely by the applied power waveform.
5. The substrate is uniformly distributed along the reactor length.

The first assumption means that the pressure *p* is high enough for the particle mean free path to be much smaller than the smallest reactor dimension, *d*. For a typical situation this translates to *pd* > 0.5 torr-cm.

The one-dimensional approximation would be better for slow surface reactions, and for high aspect ratio (long) reactors. In such case, the species concentration gradients normal to the axis would be small compared to the axial gradients. Furthermore, in a typical situation, the flow is laminar and usually fully developed with a parabolic velocity profile. This contradicts the assumption of flat velocity profile. However, the effect of velocity variations over the reactor cross section may be accounted for by using the appropriate dispersion coefficient (19). For the low

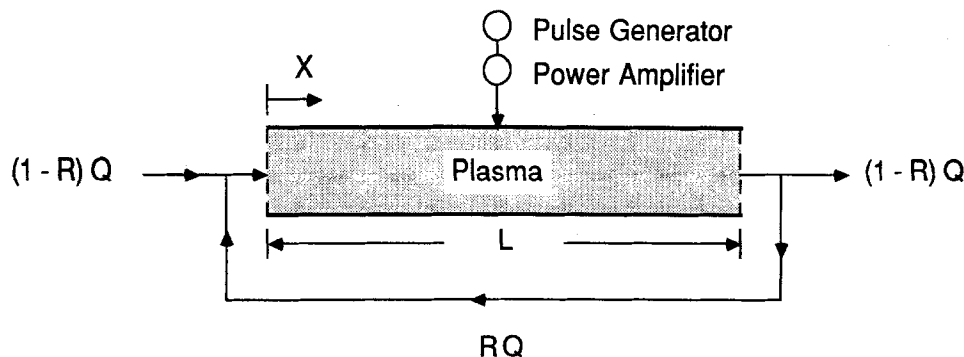


Fig. 1. Schematic of a plasma-assisted CVD reactor with recycle.

pressures of interest, the dispersion coefficient is approximately equal to the species diffusivity.

The third assumption implies a negligible pressure drop along the reactor and a thermal conductivity high enough to maintain a uniform temperature in the gas and along the reaction surface. However, the gas and the surface may be at different temperatures. The isochoric assumption implies a negligible change in the number of moles due to reaction. Therefore, the linear gas velocity is constant along the reactor length. This assumption will be valid under conditions of high dilution in an inert gas. For example, during plasma deposition of silicon from silane, a high dilution in helium or argon is used to avoid gas-phase nucleation and formation of powder. Under such conditions, multicomponent diffusion effects may be neglected, and a pseudobinary diffusion coefficient may be used to describe species transport.

The fourth assumption means that the electron density and energy follow the time dependence of the applied waveform. More complex electron density waveforms which may arise because of electron attachment (14) were not considered. The electron energy distribution function is expected to be completely modulated when the electron energy relaxation frequency is much higher than the pulsing frequency. For typical conditions, the former is in the 10-100 MHz range, much higher than the pulsing frequencies of interest (1-1000 Hz). For modeling purposes, the fourth assumption essentially implies that the overall rate constant of the electron-impact dissociation reaction [R-1] ($k_p n_e$, see Eq. [3] below) follows exactly the applied waveform.

Using the above assumptions, the material balance equation for the main radical A ($i = 1$) and the precursor species AB ($i = 2$) becomes

$$\frac{\partial c_i}{\partial t} + u \frac{\partial c_i}{\partial x} = D_i \frac{\partial^2 c_i}{\partial x^2} + G_i \quad [2]$$

where c_i and D_i are concentration and diffusivity of species i , respectively, u is the average fluid velocity, x is axial coordinate, and t is time. The net generation term G_i becomes

$$G_1 = k_p n_e c_2 - \left(\frac{S}{V}\right)_n k_n c_1 - k_v c_1^2 c_M \quad [3]$$

$$G_2 = -k_p n_e c_2 \quad [4]$$

where k_p , k_n , and k_v are the rate constants for reactions [R1], [R2], and [R3], respectively, n_e is the electron density, and c_M is the uniform concentration of the inert gas (e.g., He or Ar). According to assumption 4, the product $k_p n_e$ follows exactly the temporal variations of the applied power waveform. The surface to volume ratio $(S/V)_n$ was used to transform the surface reaction term into a homogeneous reaction term as needed for the one-dimensional model. For example, for a tubular reactor in which deposition takes place throughout the reactor walls, $(S/V)_n = 2/R_i$, where R_i is the tube radius. The surface to volume ratio accounts for the reactor loading, i.e., the substrate surface area per unit reactor volume. Linear kinetics was assumed for the deposition (etching) reaction. The total gas concentration was found by using the ideal gas law

$$c = \frac{p}{R_g T_g} \quad [5]$$

where p is the reactor pressure, and R_g and T_g are the universal gas constant and the gas temperature, respectively. Dankwerts-type boundary conditions were applied to Eq. [2] including recycle (20)

$$\text{At } x = 0, -D_i \frac{\partial c_i}{\partial x} = -u c_i|_{x=0} + u[(1-R)c_{iF} + R c_i|_{x=L}] \quad [6]$$

$$\text{At } x = L, \frac{\partial c_i}{\partial x} = 0 \quad [7]$$

where c_{iF} is the species i concentration in the fresh gas stream and R is the recycle ratio defined by Eq. [1]. Boundary conditions Eq. [6] and [7] must be applied in the entire time domain in order to reach a periodic steady-state. The initial condition was

$$\text{At } t = 0, c_1 = 0 \text{ and } c_2 = c_{2F} \quad [8]$$

It is instructive to recast Eq. [2]-[8] in dimensionless form by defining the following dimensionless parameters

$$\xi = \frac{x}{L}, C_i = \frac{c_i}{c_{2F}}, T = \frac{ut}{L} = \frac{t}{\tau}, T_p = \frac{\tau_p}{\tau} \quad [9]$$

$$Da_p = \frac{k_p n_e L^2}{D_1}, Da_n = \frac{\left(\frac{S}{V}\right)_n k_n L^2}{D_1}, Da_v = \frac{k_v c_{2F}^2 L^2}{D_1} \quad [10]$$

$$Pe_i = \frac{uL}{D_i} \quad [11]$$

where τ is the species residence time in the reactor, and τ_p is the pulse period. The species concentration was made dimensionless by dividing by the precursor gas concentration in the fresh gas stream, c_{2F} . The Damkohler number Da shows the relative importance of reaction as compared to axial dispersion. Three Da numbers arise corresponding to reaction [R1] (Da_p), [R2] (Da_n), and [R3] (Da_v). The axial Peclet number Pe is a measure of convection as compared to axial diffusion. Using the above dimensionless quantities, Eq. [2]-[4] yield

$$\frac{\partial C_1}{\partial T} = \frac{1}{Pe_1} \frac{\partial^2 C_1}{\partial \xi^2} - \frac{\partial C_1}{\partial \xi} + \frac{1}{Pe_1} [Da_p(T)C_2 - Da_n C_1 - Da_v C_1^2 C_M] \quad [12]$$

$$\frac{\partial C_2}{\partial T} = \frac{1}{Pe_2} \frac{\partial^2 C_2}{\partial \xi^2} - \frac{\partial C_2}{\partial \xi} + \frac{1}{Pe_1} [-Da_p(T)C_2] \quad [13]$$

where the dependence of Da_p on time T has been emphasized.

The corresponding boundary conditions and initial condition read

$$\text{At } \xi = 0, -\frac{1}{Pe_1} \frac{\partial C_1}{\partial \xi} = -C_1|_{\xi=0} + [(1-R)C_{1F} + RC_1|_{\xi=1}] \quad [14]$$

$$\text{At } \xi = 1, \frac{\partial C_1}{\partial \xi} = 0 \quad [15]$$

$$\text{At } T = 0, C_1 = 0 \text{ and } C_2 = 1 \quad [16]$$

In a continuous-wave (CW) plasma reactor, the concentration distributions will attain a steady state after an initial transient. For the CW reactor case, only the steady state was examined in the present work. However, in a pulsed-plasma reactor, in which Da_p varies periodically with time, the concentration distributions will reach a periodic steady state after a number of cycles. For the pulsed-plasma reactor case, emphasis was placed on the periodic steady-state in the present work.

A square-wave power modulation, as shown in Fig. 2, was used as the excitation waveform for the pulsed-plasma reactor. In such case, the mathematical representation of the time dependence of Da_p can be written as

$$Da_p(T) = Da_{p0} \left[\sum_{j=0}^{N_p} [U(T - jT_p) - U(T - (j + f_d)T_p)] \right] \quad [17]$$

for $jT_p \leq T < (j+1)T_p, j = 0, 1, \dots, N_p$ where N_p is the number of pulses (cycles) and Da_{p0} corresponds to the power level P_0 during the plasma-on fraction of the cycle (Fig. 2). $U(y)$ is a step function defined as $U(y) = 1$ for $y \geq 0$ and $U(y) = 0$ for $y < 0$. The duty cycle $f_d (0 \leq f_d \leq 1)$ is given by Eq. [18] below

$$f_d = \frac{T_1}{T_p} \quad [18]$$

where T_1 is the plasma-on time during a pulse period (Fig. 2).

In order to compare the CW reactor performance with that of the pulsed-plasma reactor, the average deposition rate and uniformity were defined as

$$r_{av} = Da_n C_{1,av} = Da_n \int_0^1 C_1(\xi) d\xi \quad [19]$$

where, for the CW reactor, $C_1(\xi)$ is the steady-state concentration distribution of radicals. For the pulsed-plasma reactor $C_1(\xi)$ in Eq. [19] is replaced by $\bar{C}_1(\xi)$, the concentration distribution averaged over a pulse period, after the periodic steady state has been achieved

$$\bar{C}_1(\xi) = \frac{\int_T^{T+T_p} C_1(\xi, T) dT}{T_p} \quad [20]$$

The uniformity index was defined as

$$UI = \frac{r_{max} - r_{min}}{2r_{av}} = \frac{C_{1,max} - C_{1,min}}{2C_{1,av}} \quad [21]$$

where r_{max} , r_{min} , and r_{av} are the maximum, minimum, and average deposition rate, respectively. UI is a measure of the deposit thickness uniformity. The lower the value of UI , the better the uniformity.

Method of Solution

The system of time-dependent partial differential Eq. [12] and [13] along with the associated boundary and initial conditions Eq. [14]-[16] was solved by using the method of lines (21-23). In this method, the spatial derivatives are discretized by using finite difference or finite element approximations. Thus, the nodal values of each dependent variable become unknown functions of time. The

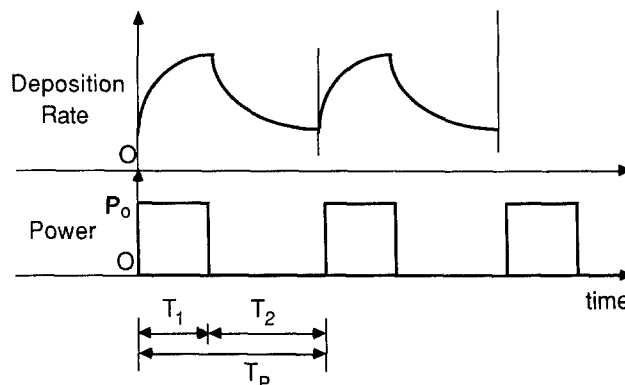


Fig. 2. Square-wave modulation of power input to the plasma, and schematic of time response of deposition rate.

resulting set of ordinary differential equations (ODE) can be solved by a variety of techniques (21-25).

A system of time dependent partial differential equations (PDE) in one spatial dimension x may be represented by

$$\frac{\partial \mathbf{C}}{\partial t} = \mathbf{F}(t, x, \mathbf{C}, \mathbf{C}_x, \mathbf{C}_{xx}, \mathbf{P}) \quad x \in [x_L, x_R], t \in [t_0, t_f] \quad [22]$$

where

$$\mathbf{C} = \{C_{i,j=1}^{NPDE}\}, \mathbf{C}_x = \{C_{xi,j=1}^{NPDE}\}, \text{ and } \mathbf{C}_{xx} = \{C_{xxi,j=1}^{NPDE}\}$$

C_i, C_{xi} , and C_{xxi} are the i th dependent variable (e.g., concentration of species i), its first derivative, and its second derivative, respectively, \mathbf{P} is a vector of parameters (e.g., Pe, Da), \mathbf{F} is a vector-valued function, x_L and x_R are the left-most and right-most point in the spatial domain, respectively; t_0 and t_f are the initial and final time, respectively, and N_{PDE} is the number of PDEs. The boundary conditions at each of the boundary points may be expressed as

$$\mathbf{B}(t, \mathbf{C}, \mathbf{C}_x) = 0, t \in [t_0, t_f] \quad [23]$$

where \mathbf{B} is a vector of dimension N_{PDE} , and \mathbf{C} and \mathbf{C}_x are evaluated at the corresponding boundary point. The initial condition can be written as

$$\mathbf{C}(t_0, x) = \mathbf{C}_0(x) \quad x \in (x_L, x_R) \quad [24]$$

where \mathbf{C} and \mathbf{C}_0 are again vectors of dimension N_{PDE} , with $\mathbf{C}_0(x)$ known. It is assumed that all functions are continuous in time and at least piecewise continuous in space.

In the present work, the spatial domain was divided into N_e elements, and each unknown dependent variable was expanded in terms of a set of piecewise B-spline basis functions (26)

$$C_i(x, t) = \sum_{j=1}^{N_b} a_{ij}(t) B_j^{kn}(x), i = 1, N_{PDE} \quad [25]$$

where N_b is the number of B-spline collocation points, B_j^{kn} is a polynomial of degree k (and $n-1$ continuity) on each element $[x_l, x_{l+1}]$, $l = 1, N_e$, with $x_1 = x_L$ and $x_{N_e+1} = x_R$; x_l and x_{l+1} define the end-points of element l , and a_{ij} is the time-dependent unknown coefficient of variable C_i at point j . This is the so-called collocation on finite elements method (22). The collocation points were chosen such that

$$x_L = x_1 = \xi_1 < \xi_2 < \dots < \xi_m < \dots < \xi_{N_b} = x_{N_e+1} = x_R \quad [26]$$

and

$$B_j^{kn}(\xi_m) = \begin{cases} 0 & \text{for } j \neq m \\ \neq 0 & \text{for } j = m \end{cases}, m = 1, 2, \dots, N_b \quad [27]$$

By substituting Eq. [25] into Eq. [22], and implementing the boundary conditions Eq. [23], leads to a system of $N_{PDE} \times N_b$ time-dependent ODEs for the components of the unknown vector \mathbf{a}

$$\mathbf{A} \frac{d\mathbf{a}}{dt} = \mathbf{f}(t, \mathbf{a}) \quad [28]$$

where **A** is a known matrix having a maximum bandwidth of $(2k \times N_{PDE} - 1)$, and **f** is a known function of *t* and **a**. The initial condition is found by substituting Eq. [25] into Eq. [24] to yield a relation of the form

$$\mathbf{a} = \mathbf{a}_0 \text{ at } t = t_0 \quad [29]$$

In the present work, the resulting set of ODEs was solved by using LSODI (23-25) with automatically variable order and variable time-step size, controlled by estimating the time discretization error. However, the maximum time-step size allowed was set to 1/10 of the pulse period. Fifty elements with cubic spline basis functions were used which led to 102 collocation points. The resulting system of 204 ODEs was solved on an NEC SX-2 supercomputer in double precision. The periodic steady state was detected by using the criterion

$$\epsilon_{\text{pss}} = \left\{ \frac{\sum_{j=1}^{N_b} \left\{ \left(\frac{r_j}{\tau_{\text{av}}} \right)_{(i+1)T_p} - \left(\frac{r_j}{\tau_{\text{av}}} \right)_{iT_p} \right\}^2}{N_b^2} \right\}^{1/2} \quad [30]$$

where r_j is the reaction rate at collocation point *j*, and ϵ_{pss} is a user-specified error tolerance. For a run using $T_p = 0.01$ and $\epsilon_{\text{pss}} = 10^{-6}$, it took 3 min of CPU time to achieve the periodic steady state. The required CPU time was most sensitive to T_p and ϵ_{pss} . The CPU time decreased as T_p or ϵ_{pss} increased.

Results and Discussion

The main quantities of interest in the present work were the reaction rate and its uniformity along the reactor axis, as a function of the system parameters. The effect of a parameter was studied by changing the value of that parameter while keeping the other parameters at their basic value. The basic values of the parameters and the range of values examined are shown in Table I. The radical diffusivity was estimated based on the deposition of silicon using a SiH_4/He mixture. For example, for a 5% SiH_4/He mixture at $p = 0.5$ torr and $T_g = 300$ K, the diffusivity is about $D_1 = 800 \text{ cm}^2/\text{s}$ (9). Assuming a reactor length $L = 50$ cm, a $\text{Pe} = 10$ corresponds to a linear gas velocity of 160 cm/s. For a flow rate of 250 sccm, this linear velocity is attained in a tubular reactor having radius $R_t = 3.72$ cm. Under these conditions, a value of $\text{Da}_p = 100$ corresponds to $k_p n_e = 32 \text{ s}^{-1}$, and a value of $\text{Da}_n = 40$ corresponds to $k_n = 23.8 \text{ cm/s}$.

For simplicity, the Peclet numbers for the precursor gas and for the radicals were set equal, which amounts to assuming equal diffusivities for these species. Results are first reported for a CW reactor, followed by the pulsed-plasma reactor. Finally the effect of recycle on both the CW and pulsed-plasma reactors is illustrated. In the discussion below, the parameters were at their basic value unless noted otherwise. All figures shown below are in terms of dimensionless quantities. For the pulsed-plasma reactor, the values of Da_p given below correspond to Da_p of Eq. [17].

For given reactor dimensions, the Da_n number cannot be arbitrarily high. For example, when the surface reaction is very rapid, the deposition rate will be limited by diffusion of radicals to the reactor walls. In such case, the "rate constant" $(S/V)_n k_n = D_1/\Lambda^2$ where Λ is the characteristic radi-

cal diffusion length. For example, for a tubular reactor having radius R_t , $\Lambda = R_t/2.405$. Thus, for a tubular reactor of aspect ratio (L/R_t) , the maximum value of Da_n will be $\text{Da}_n = (2.405)^2 (L/R_t)^2 = 5.784 (L/R_t)^2$.

Continuous-wave (CW) plasma reactor.—By neglecting the nonlinear term ($\text{Da}_v = 0$), an analytic solution may be found for the system of Eq. [12] and [13] subject to the linear boundary conditions Eq. [14]–[16]. However, even for the simplified case of time-invariant reactor operation (CW reactor), the resulting expressions are extremely cumbersome. An analytic solution was obtained for the CW reactor ($\partial C_i/\partial T = 0$) with recycle, by employing standard linear operator theory (20, 27). The solution, shown in Appendix A, was used to test the numerical solution. Several cases were tested including recycle. In all cases, the numerical solution differed from the analytic solution by less than 0.1%.

Figure 3a shows the concentration distribution of the precursor gas (C_2) for a CW reactor and for different values of the Peclet number, Pe . In practice, an increase (decrease) in Pe may be accomplished by increasing (decreasing) the gas flow rate. For a given Pe , the precursor gas concentration decreases monotonically along the reactor, due to electron-impact dissociation in the plasma (reaction [R1]). For low values of Pe , a discontinuity in C_2 ($C_2(0^-) = 1$ but $C_2(0^+) < 1$) is observed at the reactor entrance due to species reaction and back diffusion. For the parameter values examined and for $\text{Pe} < 10$, there is complete conversion of the precursor gas. For very high values of Pe (very high flow rates), the gas residence time becomes very short and the chance for dissociation diminishes. Therefore, the precursor gas concentration does not change appreciably along the reactor length (case of $\text{Pe} = 1000$). In such case, the gas is not utilized efficiently, since most of the gas passes through the reactor unconverted.

The concentration (C_1) profiles for the reactive radical are shown in Fig. 3b, for the same parameter values as in Fig. 3a. Since the reaction rate was assumed proportional to C_1 , Fig. 3b shows the relative reaction rate and uniformity distributions as well. For low values of Pe (e.g., $\text{Pe} = 1$), C_1 decreases monotonically due to strong depletion of the precursor gas (see Fig. 3a). For higher Pe , a maximum appears in the radical concentration profile. This maximum can be explained as follows: close to the reactor entrance, the rate of radical production by reaction [R1] exceeds its rate of consumption by reaction [R2]. Therefore the radical concentration builds up. Further downstream however, the rate of radical production decreases because of precursor gas depletion. Therefore, the radical is consumed faster than it is produced, resulting in a decrease in the radical concentration. Hence, a maximum in radical concentration develops. Intuitively, the rates of radical production and loss must be equal at the location of the maximum. The existence and location of the maximum depend on the parameter values. For example, as Pe increases, the location of the maximum shift downstream, and at sufficiently high Pe (e.g., $\text{Pe} > 100$ in Fig. 3b) there is no maximum. In the latter case, the radical concentration increases monotonically with reactor length. The existence of a maximum in the axial deposition rate has been observed experimentally in plasma deposition (8, 9) and in plasma polymerization (6).

The effect of the Damkohler number for radical production Da_p is shown in Fig. 4. Da_p may be increased (decreased) by increasing (decreasing) the power delivered to the plasma. Figure 4a shows the concentration distribution of the precursor gas, C_2 . For a given Da_p , C_2 decreases monotonically along the reactor length. As Da_p increases, the degree of precursor gas dissociation increases resulting in lower gas concentration and higher conversion at the reactor exit. The corresponding concentration profiles for the radicals are illustrated in Fig. 4b. As Da_p increases, the spatially averaged radical concentration increases, but the concentration profile becomes strongly nonuniform. Furthermore, as Da_p increases, the maximum in the concentration profile shifts towards the reactor inlet, and the decrease in concentration after the maximum becomes steeper. This is a result of precursor gas depletion becom-

Table I. Dimensionless parameters and values used for calculation

Parameter	Name	Basic value	Range examined
Pe	Peclet number	10	1-1000
Da_p	Damkohler number for radical production	100	1-100
Da_n	Damkohler number for deposition	40	1-250
Da_v	Damkohler number for volume recombination	0	—
T_p	Dimensionless pulse period	0.1	0.001-10
f_d	Duty cycle	50%	0%-100%
R	Recycle ratio	0	0-0.9

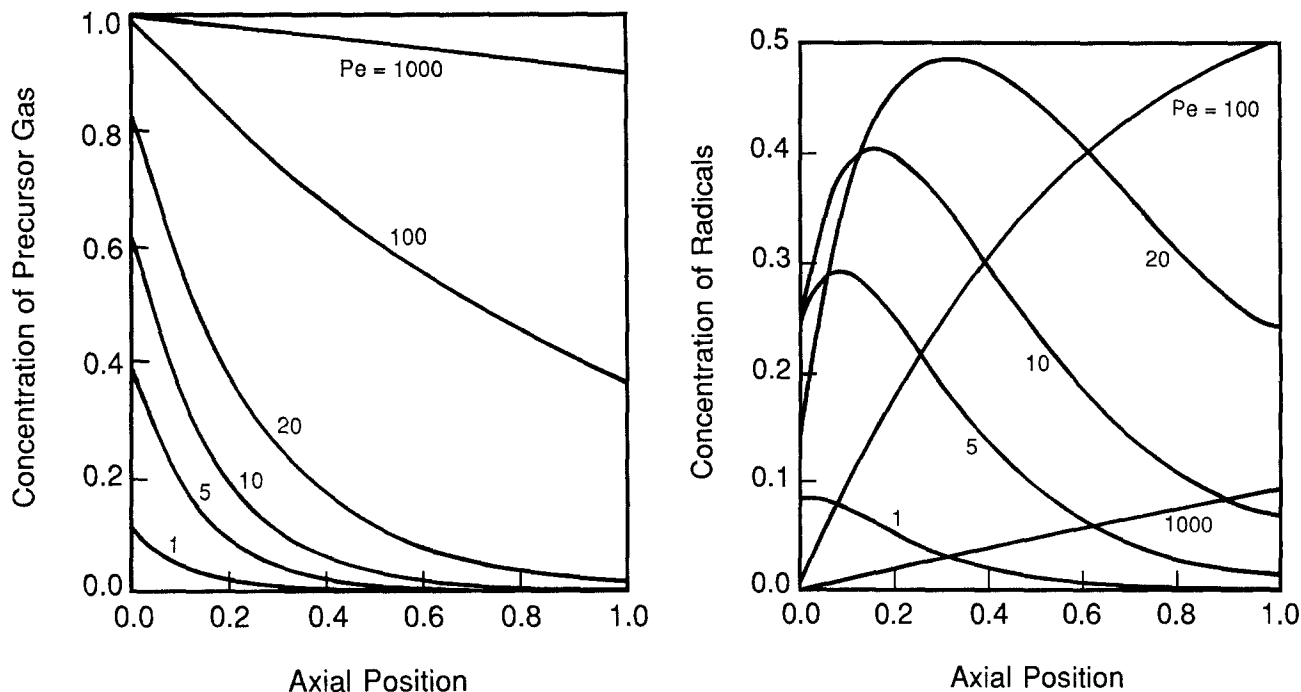


Fig. 3. (a, left) Dimensionless concentration of precursor gas as a function of axial position for a CW reactor without recycle, with the Pe number as a parameter. $Da_p = 100$, $Da_n = 40$. (b, right) Dimensionless radical concentration as a function of axial position for a CW reactor without recycle. Parameter values as in (a).

ing stronger with increasing Da_p , which in turn results in reduced rate of radical production. One observes that by increasing Da_p (power to the system), the average deposition rate increases but the deposit uniformity degrades. This is true for low Peclet numbers. For high Peclet numbers ($Pe > 25$) the deposit uniformity was found to improve (lower UI) with increasing Da_p .

The spatially averaged deposition rate is shown in Fig. 5 as a function of the Peclet number with Da_p as a parameter. For a given value of Pe, the reaction rate increases with increasing Da_p (increasing power into the plasma). For a given value of Da_p , when Pe is low (low flow rate), the rate is limited by the supply of precursor gas which is completely converted in the reactor. When Pe is high (high flow rate), the rate is limited by insufficient precursor gas

dissociation and by convective removal of the radical species. Therefore, the rate is maximum at an intermediate value of Pe. The position of the maximum depends on the other parameter values. For example, the maximum shifts to higher Pe as Da_p increases. Similar behavior with flow rate has been observed for purely chemical etching in radial flow parallel-plate plasma reactors (18) and in plasma-assisted downstream etching reactors (28).

The uniformity index (UI) was calculated as a function of the Peclet number (in the range 5-200) for different values of Da_p (in the range 1-100), and for a value of $Da_n = 40$. For low values of Da_p (e.g., $Da_p < 1$), UI increased monotonically with increasing Pe. For high values of Da_p (e.g., $Da_p > 5$), UI first decreased sharply with increasing Pe, reached a minimum (around $Pe = 10$, depending on the

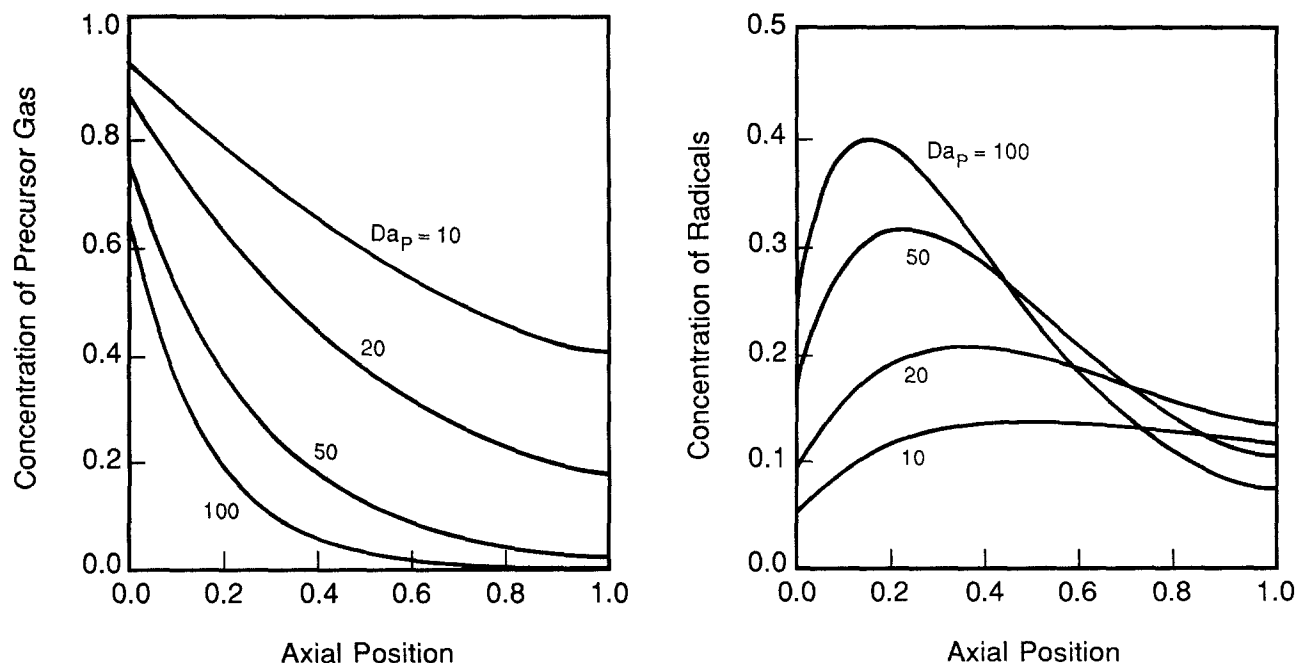


Fig. 4. (a, left) Dimensionless concentration of precursor gas as a function of axial position for a CW reactor without recycle, with the Da_p number as a parameter. $Pe = 10$, $Da_n = 40$. (b, right) Dimensionless radical concentration as a function of axial position for a CW reactor without recycle. Parameter values as in (a).

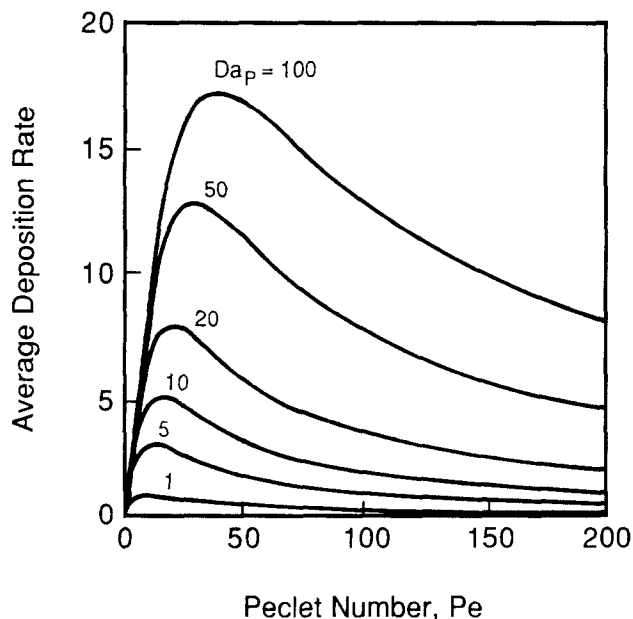


Fig. 5. Spatially averaged deposition rate as a function of the Pe number with the Da_p number as a parameter, for a CW reactor without recycle and for $Da_n = 40$.

value of Da_p), and then increased monotonically with further increase in Pe. The uniformity index as a function of the Peclet number for $Da_p = 100$, and for different values of Da_n (in the range 2.5-250) showed similar behavior (*i.e.*, *UI* passed through a minimum). The average deposition rate as a function of the Peclet number for $Da_p = 100$, and for different values of Da_n (in the range 2.5-250) showed behavior very similar to that of Fig. 5. Finally, for given values of Pe and Da_p , the average deposition rate increased monotonically with increasing Da_n reaching a plateau for sufficiently high values of Da_n (for $Da_n > 100$, when Pe was 10 and Da_p was in the range 1-100). The deposition rate at the plateau was limited by radical production.

Pulsed-plasma reactor.—There are numerous studies in the chemical engineering literature on the dynamic behavior of chemical reactors under a periodic excitation (29). However, in these studies the reactor is usually excited by varying the inlet flow rate or the inlet reactant concentration or temperature. In conventional chemical reactors, it is very difficult to vary the reaction rate constant in a predetermined manner, since reactions are thermally activated and the system has a relatively long thermal response time. Modulation of the reaction rate constant can be readily achieved in plasma reactors for reactions, such as electron-impact dissociation, which depend on the electron energy and density. In this respect, the pulsed-plasma reactor system considered here differs from the conventional pulsed chemical reactor systems. Electrochemical reactors comprise another class of systems in which the reaction rate constant (or reaction rate) may be modulated according to a given waveform, by modulating the potential (or current) applied to the cell (30).

The spatial and temporal distribution of the deposition rate is shown in Fig. 6 for a pulsed-plasma reactor. This plot corresponds to the periodic steady-state achieved after a number of cycles. Parameters were at their basic value (Table I) except that the dimensionless pulse period $T_p = 1$, *i.e.*, the pulse period was equal to the species residence time in the reactor. As expected, the deposition rate increases during the plasma-on fraction of the cycle, and decreases during the plasma-off fraction of the cycle. The decay time is determined by the radical loss mechanisms such as convective flow and deposition. One observes that deposition continues well after plasma extinction. This is the case when the plasma-off fraction of the cycle is not much longer than the radical lifetime.

The radical concentration (and reaction rate) distribution along the reactor is shown in Fig. 7 for different values of the duty cycle. The curve corresponding to CW opera-

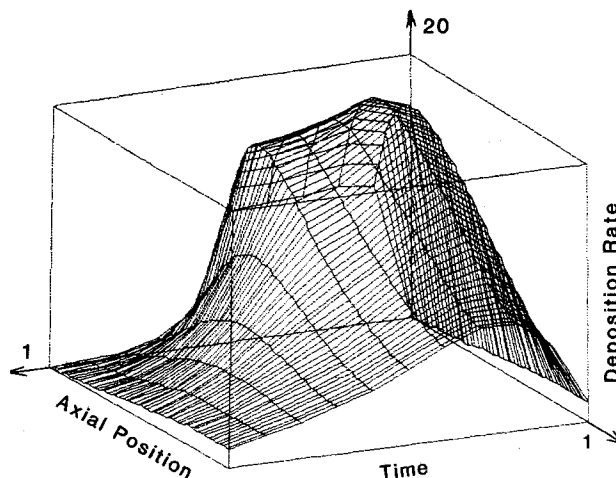


Fig. 6. Spatial and temporal variation of the dimensionless deposition rate in a pulsed-plasma reactor without recycle, after the periodic steady-state has been reached. $Pe = 10$, $Da_p = 100$, $Da_n = 40$, $T_p = 1$, duty cycle = 50%. Time is plotted as a fraction of the pulse period.

tion (100% duty cycle) is also shown. When compared to CW operation, pulsed-plasma operation has the effect of decreasing the reaction rate near the reactor inlet, and increasing the rate near the exit. The result is a smoother reaction rate distribution and improved uniformity. The effect is more pronounced for lower values of the duty cycle. However, the average reaction rate decreases with duty cycle. Hence, by controlling the duty cycle, better uniformity may be obtained at the expense of throughput.

A comment is in order at this point. A "smoother" radical concentration profile does not necessarily imply improved uniformity (lower uniformity index *UI*). This is because the average deposition rate, τ_{av} (Eq. [19] and [20]) is used in the denominator of Eq. [21] defining the *UI*. Thus, if the smoother concentration profile (smaller value of $\tau_{max} - \tau_{min}$) is accompanied by a sufficient reduction in τ_{av} , the uniformity (as defined by the *UI*) may be worse, even though the deposition rate profile is smoother.

The pulsed-plasma effect on reaction uniformity can be understood by examining Fig. 8, which shows the precursor gas concentration (C_2) distribution in the reactor for

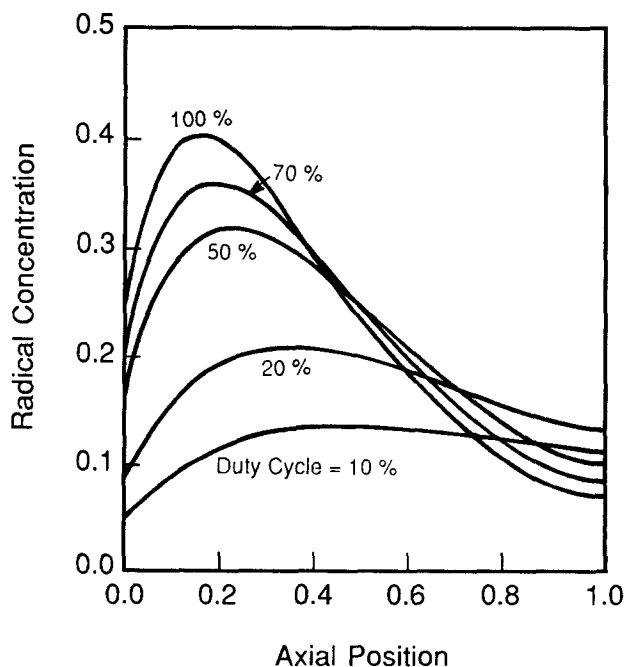


Fig. 7. Dimensionless radical concentration as a function of axial position in a pulsed-plasma reactor without recycle, with the duty cycle as a parameter. $T_p = 0.1$, $Pe = 10$, $Da_p = 100$, $Da_n = 40$.

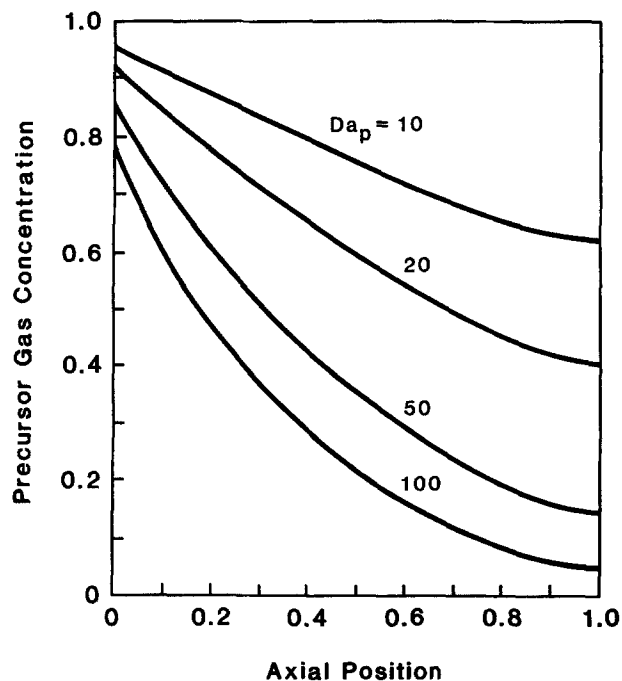


Fig. 8. Dimensionless concentration of precursor gas as a function of axial position for a pulsed-plasma reactor without recycle, with the Da_p number as a parameter. $T_p = 1$, $Pe = 10$, $Da_n = 40$, duty cycle = 50%.

$T_p = 1$ and a duty cycle of 50%. Other parameter values were as in Fig. 4a. By comparing to the CW reactor case (Fig. 4a), one observes that pulsing the plasma diminishes the depletion of the precursor gas which occurs in the CW reactor, especially for large values of Da_p , and small values of Pe (not shown in the figure). In essence, the reactor is allowed to be "refilled" with fresh gas during the plasma-off fraction of the cycle. Since depletion of the precursor gas can lead to deposition rate nonuniformity, pulsing the plasma can result in improved uniformity. However, since radical production takes place only during a fraction of the deposition time, pulsing the plasma yields lower average deposition rate.

The effect of pulse period and duty cycle on the spatially and temporally averaged reaction rate (Eq. [19] and [20]) is illustrated in Fig. 9. The reaction rate decreases with decreasing duty cycle, owing to reduced time-averaged production of radicals. For a given duty cycle, the reaction rate attains limiting values for very low and very high values of the pulse period. For very low pulse periods (high pulsing frequencies), the species concentration profiles cannot follow the rapidly changing applied waveform. Thus, an almost time-invariant concentration profile is reached which is not affected by further reducing the pulse period. For very large pulse periods, the system reaches the corresponding CW state in a very small fraction of the plasma-on time. Likewise, the activated gas decays during a very small fraction of the plasma-off time. Therefore, the system behavior is that of the CW state pro-rated by the duty cycle. For example, for a duty cycle of 50%, and for very high pulse periods ($T_p > 10$ in Fig. 9), the average reaction rate in the pulsed-plasma reactor is 50% of that in the CW reactor, under otherwise identical conditions. One further observes in Fig. 9 that the pulsed-plasma reactor behavior changes dramatically by pulsing on a time scale which is comparable to the characteristic time scales of the process (dimensionless pulse periods between 0.1 and 10).

The effect of pulse period and duty cycle on the deposition uniformity is shown in Fig. 10. Other parameters were at their basic value. Under these conditions, the uniformity index (Eq. [21]) for the CW reactor was 0.707. An identical UI is achieved in the pulsed-plasma reactor at high pulse periods, regardless of the duty cycle. For not so high pulse periods, the uniformity is improved by pulsing the plasma (lower uniformity index) and the improvement is

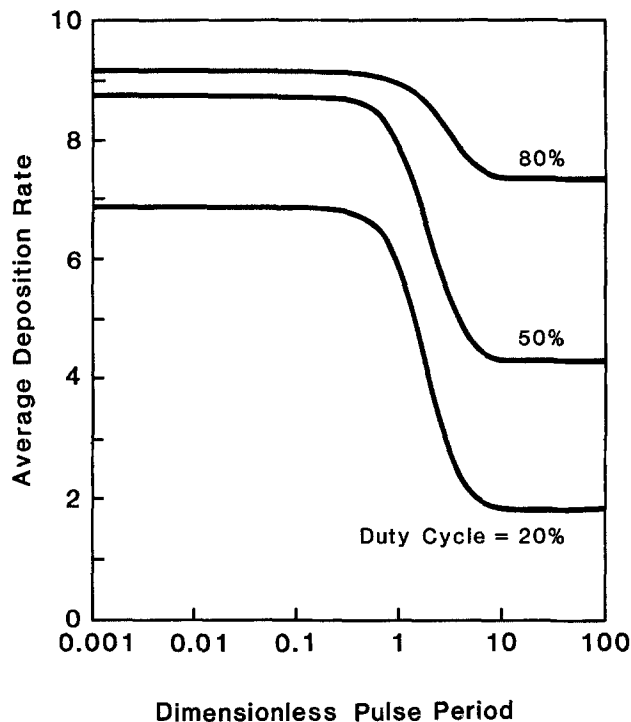


Fig. 9. Spatially and temporally averaged deposition rate in a pulsed-plasma reactor without recycle as a function of pulse period T_p with the duty cycle as a parameter. $Pe = 10$, $Da_p = 100$, $Da_n = 40$.

generally better for lower duty cycles. For very low pulse periods, the uniformity index attains a limiting value for the same reason the average deposition rate attains a limiting value for small T_p (Fig. 9). One observes in Fig. 10 that the uniformity index changes rapidly over the range of T_p values that result in rapid change of the deposition rate as well (Fig. 9). Furthermore, for a given duty cycle, there is a value of the pulse period which minimizes the uniformity index and therefore maximizes the deposition uniformity.

Further examination of Fig. 9 and 10 reveals that by using a pulsed-plasma, the deposition uniformity may be improved substantially with only a small reduction in deposition rate. For example, for a duty cycle of 50% and

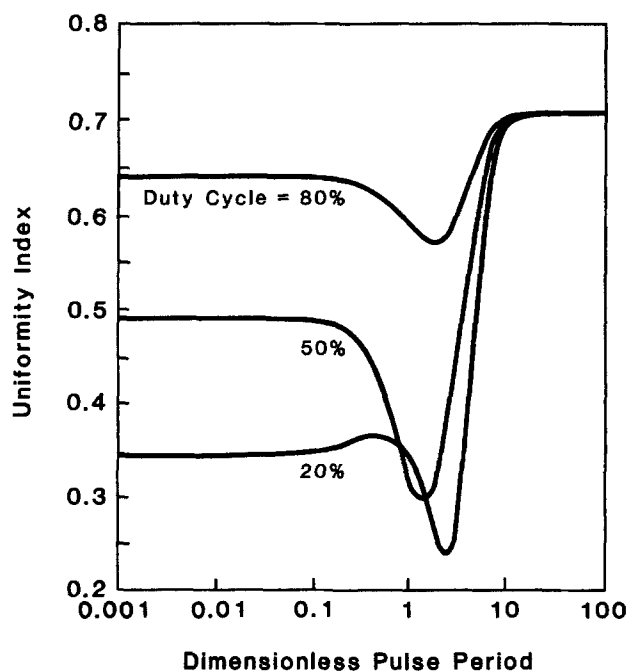


Fig. 10. Uniformity index in a pulsed-plasma reactor without recycle as a function of pulse period T_p with the duty cycle as a parameter. $Pe = 10$, $Da_p = 100$, $Da_n = 40$.

for $T_p < 0.1$, the deposition rate is reduced by only 5.9% compared to the CW case, whereas the uniformity is improved by 30% (UI is reduced from 0.71 to 0.49).

The uniformity index as a function of the Peclet number is shown in Fig. 11 for the CW reactor and for two pulse periods of the pulsed-plasma reactor. Other parameters were at their basic value. One observes that the pulsed-plasma reactor is advantageous (improved uniformity) at relatively low values of the Peclet number ($Pe < 20$). Under such condition, the precursor gas is severely depleted as the gas flows through the plasma (see Fig. 3a). At high Pe , the CW and pulsed-plasma reactors yield comparable uniformity. However, high values of Pe result in poor utilization of the reactant gas.

The present model is based on the assumption that the electron density and energy are modulated completely by the applied waveform, i.e., the plasma ignites and extinguishes instantaneously when the power is turned on and off (Fig. 2). However, for very low values of the pulse period (e.g., when the pulse frequency approaches the RF excitation frequency), this assumption may not be valid. An electron density and/or energy balance is then necessary in order to solve the problem. Such complicating factors were not examined in this work.

The effect of duty cycle on the average deposition rate is shown in Fig. 12, with the pulse period T_p as a parameter. Duty cycle values of 0 and 100% correspond to no plasma and CW operation, respectively. For small pulse periods, the average deposition rate rises steeply with duty cycle and reaches values close to the CW reactor for relatively low duty cycle values. As the pulse period increases, the duty cycle has to increase as well in order to achieve a deposition rate which is a given fraction of the CW rate.

Reactors with recycle.—Recycle has been used extensively in the chemical industry in tubular or packed bed reactors to achieve more efficient use of reactants, to control reactor temperature, and to enhance reaction selectivity (31). Recycle is equivalent to having a higher degree of back-mixing in the reactor, resulting in smoother concentration and temperature gradients. In fact, when the recycle ratio approaches unity, complete mixing results in uniform concentration and temperature in the reactor (CSTR limit). The use of recycle was shown to improve interwafer deposition uniformity in a low-pressure chemical vapor deposition (LPCVD) system (32). A disadvantage of using a recycle stream in deposition or etching systems may be contamination by particulates formed in such systems

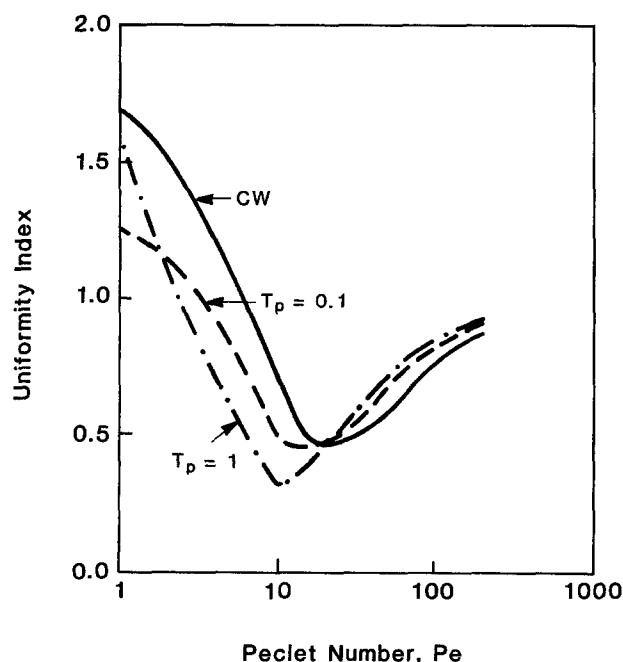


Fig. 11. Uniformity index in a CW or pulsed-plasma reactor without recycle as a function of the Peclet number Pe . $Da_p = 100$, $Da_n = 40$, duty cycle for pulsed-plasma 50%.

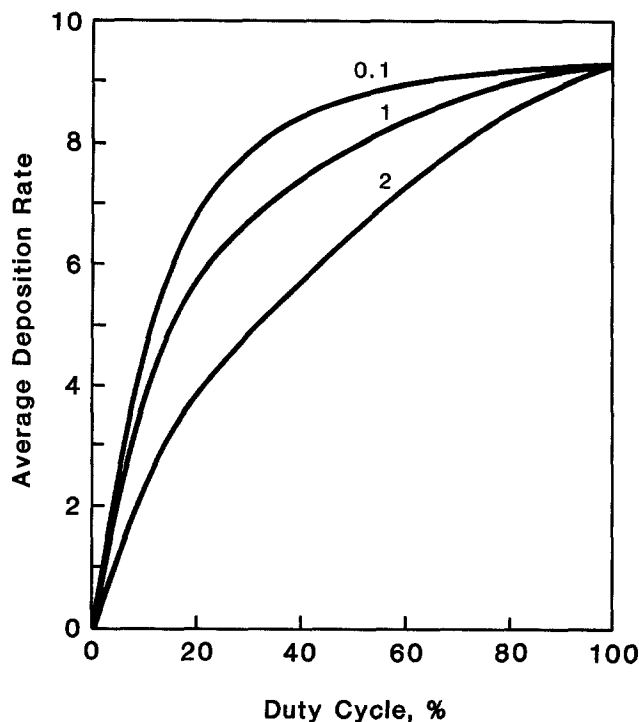


Fig. 12. Spatially and temporally averaged deposition rate in a pulsed-plasma reactor without recycle as a function of duty cycle with the pulse period as a parameter. $Pe = 10$, $Da_p = 100$, $Da_n = 40$.

which are carried with the effluent stream and are then recycled to the reactor entrance.

In the present study, the effect of recycle on the deposition rate and uniformity was studied for both CW and pulsed-plasma reactors. The following (rather severe) assumptions were made for the reactor with recycle:

1. The radicals do not react in their transit from the reactor exit to the inlet.
2. The gas is recycled instantaneously.
3. The properties of the glow discharge (such as electron density and energy) are not influenced significantly by the recycle.

Figure 13 illustrates the effect of recycle ratio on the average deposition rate for a CW reactor and for different values of Da_p . Other parameters were at their basic value (Table I) except that $Da_n = 10$. For large values of Da_p (e.g., $Da_p > 20$), the deposition rate diminishes monotonically with recycle ratio. The effect is stronger the larger the Da_p value. This can be understood by the dilution of the gas stream as a result of recycle. At high values of Da_p , the precursor gas is completely exhausted as it passes through the plasma (Fig. 4a), and the radical concentration at the reactor exit is relatively low (Fig. 4b). Hence, the recycle stream is relatively devoid of reactive species resulting in a decrease in the average radical concentration, and in turn in the average deposition rate. However, for low values of Da_p , the precursor gas concentration at the reactor exit is still high, and the radical concentration at the exit may be higher than the average radical concentration (for example, when the radical reactivity is low, in which case the radical concentration increases with axial position). In such case, recycle increases the average deposition rate as seen in Fig. 13 for $Da_p = 1$. For high radical reactivity, the average deposition rate again decreases monotonically with recycle. In summary, from the viewpoint of deposition rate, recycle is not expected to be beneficial in cases for which the radical and/or the precursor gas effluent concentrations are very small. Such cases are encountered for small Pe and large Da_n and/or Da_p .

In Fig. 14 the radical concentration (and deposition rate) distribution for a CW reactor without recycle (curve A) is compared to a pulsed-plasma reactor without recycle (curve B), to a CW reactor with recycle (curve C), and to a pulsed-plasma reactor with recycle (curves D and E). Conditions are shown in the figure caption. One observes that

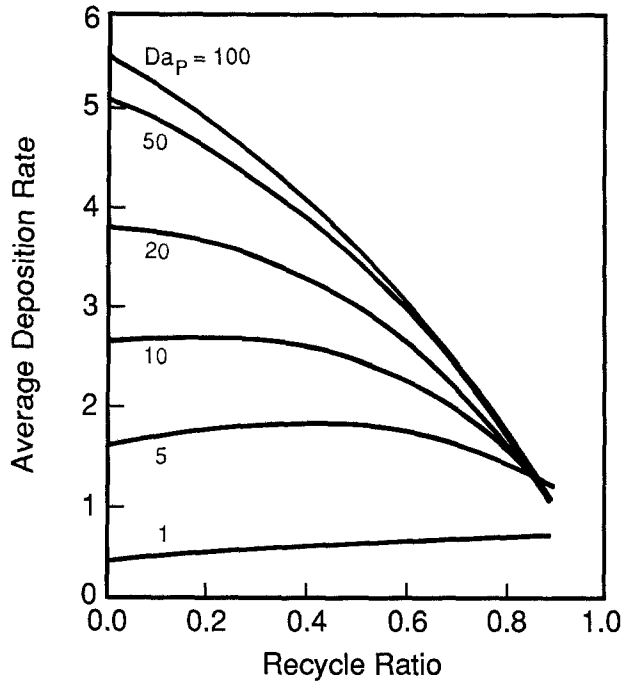


Fig. 13. Spatially averaged deposition rate as a function of recycle R in a CW reactor, with the Da_p number as a parameter. $Pe = 10$, $Da_n = 10$.

pulsed-plasma alone improves the deposition uniformity, albeit at the expense of deposition rate (compare curves A and B). A recycle stream in the CW reactor results in smoother deposition profile but lower deposition rate (curves A and C). A combination of pulsed-plasma and recycle results in even better uniformity than pulsed-plasma or recycle alone, but even lower deposition rate. This effect is stronger for smaller values of the duty cycle (curves D and E).

However, depending on the reactor operating conditions (e.g., flow rate), a combination of pulsed-plasma with recycle can be used to substantially improve the deposition

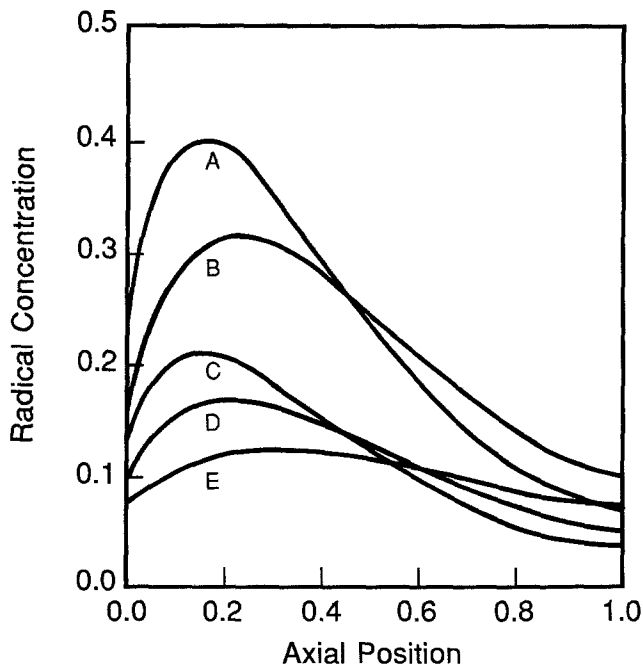


Fig. 14. Dimensionless radical concentration as a function of axial position. $Pe = 10$, $Da_p = 100$, $Da_n = 40$. Curve A: CW reactor, $R = 0$. B: pulsed-plasma reactor, $T_p = 0.1$, duty cycle = 50%, $R = 0$. C: CW reactor, $R = 0.5$. D: pulsed-plasma reactor, $T_p = 0.1$, duty cycle = 50%, $R = 0.5$. E: pulsed-plasma reactor, $T_p = 0.1$, duty cycle = 20%, $R = 0.5$.

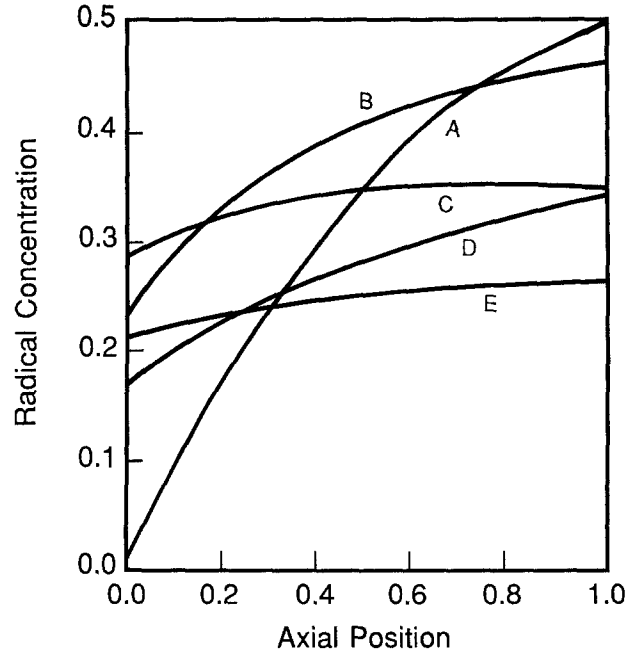


Fig. 15. Dimensionless radical concentration as a function of axial position. $Pe = 100$, $Da_p = 100$, $Da_n = 40$. Curve A: CW reactor, $R = 0$. B: CW reactor, $R = 0.5$. C: CW reactor, $R = 0.8$. D: pulsed-plasma reactor, $T_p = 0.1$, duty cycle = 50%, $R = 0.5$. E: pulsed-plasma reactor, $T_p = 0.1$, duty cycle = 50%, $R = 0.8$.

uniformity without a significant reduction of the deposition rate. This is shown in Fig. 15, for which parameter values were as in Fig. 14 except that $Pe = 100$. Here the case of CW reactor without recycle (curve A) is compared to the CW reactor with recycle (curves B and C), and to the pulsed-plasma reactor with recycle (curves D and E). In this case, recycle improves uniformity dramatically (compare curves A and B), especially at higher recycle ratios (curves B and C). The average deposition rate increases as well. Using a CW or a pulsed-plasma reactor in combination with recycle can result in nearly uniform deposit without sacrificing the deposition rate (curves A and E).

Summary and Conclusions

A one-dimensional axial dispersion model for a time-dependent plasma-assisted chemical vapor deposition reactor was developed. Transport and reaction of a precursor gas and of radicals resulting from the precursor gas dissociation in the plasma were included. The resulting model equations were solved by the method of lines using collocation on finite elements for the spatial discretization. Emphasis was placed on the effect of operating conditions on the deposition rate and uniformity (as described by the uniformity index, Eq. [21]) along the reactor axis. Under similar assumptions, the same model can describe the etching rate and uniformity in plasma reactors in which chemical etching dominates (negligible ion-assisted etching).

Three situations were examined: (i) the time-invariant steady-state achieved in a continuous wave (CW) reactor, (ii) the periodic steady-state achieved in a pulsed-plasma reactor, and (iii) the effect of recycle on the performance of the above CW and pulsed-plasma reactors. The parameter range examined is shown in Table I. Moreover, analytic solutions were derived for a CW reactor with recycle, and for a well-mixed pulsed-plasma reactor.

In the CW reactor, depletion of the precursor gas was observed for low flow rate (Pe) and/or high power into the plasma (Da_p), as expected. Such depletion can result in highly nonuniform deposition rate. The average deposition rate increased as Da_p increased, but the deposition uniformity degraded (for low Pe). A maximum in the axial deposition rate was typically observed, and this maximum shifted further downstream as Pe increased, or Da_p decreased, or Da_n (radical sticking coefficient) decreased. For given Da_p and Da_n , the deposition rate increased with Pe at

low values of Pe, reached a maximum, and then decreased with Pe.

In the pulsed-plasma reactor, the precursor-gas depletion was minimized by allowing the reactor to "refill" with fresh gas during the plasma-off fraction of the cycle. This resulted in smoother deposition rate profiles and, in general, improved uniformity. However, the average deposition rate was reduced because radical production occurred for only a fraction of the time. The average deposition rate achieved limiting values for very small and very large values of the pulse period. The average rate was very sensitive to the pulse period τ_p for values of τ_p comparable to the characteristic time scales of the system, such as the gas residence time. For given pulse period, the average deposition rate decreased as the duty cycle decreased, although the deposition uniformity generally improved. It was found that, by selecting appropriate values of the pulse period and duty cycle, uniformity may be substantially improved without significant loss of the deposition rate.

Adding a recycle stream to the CW reactor generally improved the deposition uniformity at the expense of deposition rate. Use of a recycle stream was not beneficial under conditions of high depletion of the precursor gas and high reactivity of the radicals. However, under conditions of low depletion of the precursor gas and/or low reactivity of the radicals, recycle can result in improvements in both deposition rate and uniformity.

From the above discussion it is evident that pulsed-plasma operation is most beneficial under conditions of high depletion of the precursor gas, and that the recycle stream is most beneficial under conditions of low depletion of the precursor gas. For intermediate cases, a combination of pulsed-plasma and recycle may be most useful. In fact, for given gas flow rate, radical production rate, and radical reactivity (sticking coefficient), judicious selection of the pulse period, duty cycle and degree of recycle, can result in nearly uniform deposit without sacrificing the deposition rate.

The present model is only a simplification of a real deposition (or etching) system. However, it was felt that the essential features of pulsed-plasma operation were captured. New and useful insight was provided on the complex effect of pulse period, duty cycle and recycle ratio on the deposition rate and uniformity achieved in pulsed-plasma reactors.

Acknowledgments

This work was supported by the National Science Foundation (CBT-8708908), and by the Welch Foundation. An NEC SX-2 supercomputer-time grant was provided by the Houston Area Research Center (HARC). S.-K. Park was partially supported by a scholarship from the Ministry of Education, Republic of Korea.

Manuscript submitted Sept. 5, 1989; revised manuscript received ca. Jan. 30, 1990.

The University of Houston assisted in meeting the publication costs of this article.

APPENDIX A

Steady-State Axial Dispersion Model with Recycle

An analytic solution to the steady-state ($\partial C_i/\partial T = 0$) form of Eq. [12] and [13] subject to boundary conditions Eq. [14] and [15] is presented in this Appendix. A time-independent Da_p and linear kinetics ($Da_v = 0$) was assumed. The solution was obtained using standard linear operator theory (20, 27). The solution is expressed in terms of the parameters Pe_1 , Pe_2 , Da_p , Da_n , and R . Two cases were examined depending on the parameter values.

1. For $Pe_1 \neq Pe_2$ or $\alpha \neq \beta$ (α and β are defined below) the dimensionless concentration distribution of radicals is given by

$$C_1(\xi) = d_1 \exp\left[\frac{(1-\beta)Pe_1}{2}\xi\right] + d_2 \exp\left[\frac{(1+\beta)Pe_1}{2}\xi\right] + B_1 \exp\left[\frac{(1-\alpha)Pe_2}{2}\xi\right] - B_2 \exp\left[\frac{(1+\alpha)Pe_2}{2}\xi\right]$$

where

$$\alpha = \left(1 + \frac{4Da_p}{Pe_1Pe_2}\right)^{1/2}, \quad \beta = \left(1 + \frac{4Da_n}{Pe_1^2}\right)^{1/2}$$

$$d_1 = \frac{2}{E_1Pe_1} \left[S_1(\beta + 1) \exp\left(\frac{Pe_1\beta}{2}\right) - S_2\left(\beta - 1 + 2R \exp\left(\frac{Pe_1(1+\beta)}{2}\right)\right) \right]$$

$$d_2 = \frac{2}{E_1Pe_1} \left[S_1(\beta - 1) \exp\left(\frac{-Pe_1\beta}{2}\right) - S_2\left(\beta + 1 - 2R \exp\left(\frac{Pe_1(1-\beta)}{2}\right)\right) \right]$$

$$B_1 = \frac{2Da_pC_{2F}(1-R)(1+\alpha) \exp\left(\frac{Pe_2\alpha}{2}\right)}{E_2 \left[\left(\frac{Pe_1\beta}{2}\right)^2 - \gamma_1^2 \right]}$$

$$B_2 = \frac{2Da_pC_{2F}(1-R)(1-\alpha) \exp\left(-\frac{Pe_2\alpha}{2}\right)}{E_2 \left[\left(\frac{Pe_1\beta}{2}\right)^2 - \gamma_2^2 \right]}$$

with

$$E_1 = (1+\beta)^2 \exp\left(\frac{Pe_1\beta}{2}\right) - (1-\beta)^2 \exp\left(\frac{-Pe_1\beta}{2}\right) - 4R\beta \exp\left(\frac{Pe_1}{2}\right)$$

$$E_2 = (1+\alpha)^2 \exp\left(\frac{Pe_2\alpha}{2}\right) - (1-\alpha)^2 \exp\left(\frac{-Pe_2\alpha}{2}\right) - 4R\alpha \exp\left(\frac{Pe_2}{2}\right)$$

$$\gamma_1 = \frac{Pe_2(1-\alpha) - Pe_1}{2}, \quad \gamma_2 = \frac{Pe_2(1+\alpha) - Pe_1}{2}$$

$$S_1 = \left[(1-R)Pe_1C_{1F} + RPe_1 \exp\left(\frac{Pe_1}{2}\right) (B_1 \exp(\gamma_1) - B_2 \exp(\gamma_2)) - \left(\frac{Pe_1}{2} - \gamma_1\right)B_1 + \left(\frac{Pe_1}{2} - \gamma_2\right)B_2 \right]$$

$$S_2 = \left(\frac{Pe_1}{2} + \gamma_1\right)B_1 \exp(\gamma_1) - \left(\frac{Pe_1}{2} + \gamma_2\right)B_2 \exp(\gamma_2)$$

The above solution is only valid for

$$\gamma_1^2 \neq \left(\frac{Pe_1\beta}{2}\right)^2, \quad \gamma_2^2 \neq \left(\frac{Pe_1\beta}{2}\right)^2$$

The precursor gas concentration profile is given by

$$C_2(\xi) = \frac{2C_{2F}(1-R)}{E_2} \left\{ (1+\alpha) \exp\left(\frac{Pe_2\alpha}{2}\right) \exp\left(\frac{Pe_2(1-\alpha)}{2}\xi\right) - (1-\alpha) \exp\left(\frac{-Pe_2\alpha}{2}\right) \exp\left(\frac{Pe_2(1+\alpha)}{2}\xi\right) \right\}$$

2. For $Pe_1 = Pe_2 = Pe$ and $\alpha = \beta$ (i.e., $Da_p = Da_n$), $\gamma_1 = \gamma_2 = (Pe\beta/2)^2$, and the above solution is not valid. In this case the radical dimensionless concentration distribution is given by

$$C_1(\xi) = d_1 \exp\left(\frac{Pe(1-\alpha)}{2}\xi\right) + d_2 \exp\left(\frac{Pe(1+\alpha)}{2}\xi\right) + \left\{ B_1 \exp\left(\frac{Pe(1-\alpha)}{2}\xi\right) - B_2 \exp\left(\frac{Pe(1+\alpha)}{2}\xi\right) \right\} \xi$$

where

$$\alpha = \left(1 + \frac{4Da_p}{Pe^2}\right)^{1/2}$$

$$E = (1+\alpha)^2 \exp\left(\frac{Pe\alpha}{2}\right) - (1-\alpha)^2 \exp\left(-\frac{Pe\alpha}{2}\right) - 4\alpha R \exp\left(\frac{Pe}{2}\right)$$

$$B_1 = \frac{2Da_p C_{2F}(1-R)(1+\alpha) \exp\left(\frac{Pe\alpha}{2}\right)}{E Pe \alpha}$$

$$B_2 = \frac{2Da_p C_{2F}(1-R)(1-\alpha) \exp\left(-\frac{Pe\alpha}{2}\right)}{E(-Pe\alpha)}$$

$$d_1 = \frac{2}{E Pe} \left[S_1(\alpha+1) \exp\left(\frac{Pe\alpha}{2}\right) - S_2 \left(\alpha - 1 + 2R \exp\left(\frac{Pe(\alpha+1)}{2}\right) \right) \right]$$

$$d_2 = \frac{2}{E Pe} \left[S_1(\alpha-1) \exp\left(-\frac{Pe\alpha}{2}\right) - S_2 \left(\alpha + 1 - 2R \exp\left(\frac{Pe(1-\alpha)}{2}\right) \right) \right]$$

$$S_1 = (1-R)PeC_{1F} + RPe \exp\left(\frac{Pe}{2}\right) \left(B_1 \exp\left(-\frac{Pe\alpha}{2}\right) - B_2 \exp\left(\frac{Pe\alpha}{2}\right) \right) + B_1 - B_2$$

$$S_2 = \left(1 - \frac{Pe\alpha}{2} - \frac{Pe}{2}\right) B_1 \exp\left(-\frac{Pe\alpha}{2}\right) - \left(1 + \frac{Pe\alpha}{2} + \frac{Pe}{2}\right) B_2 \exp\left(\frac{Pe\alpha}{2}\right)$$

The precursor gas concentration profile remains as before.

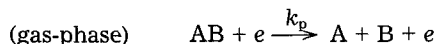
APPENDIX B

Pulsed-Plasma Well-Mixed Reactor Model

The time-dependent concentrations and deposition rate in a well-mixed pulsed-plasma reactor are presented in Appendix B. The well-mixed (continuous stirred tank reactor, CSTR) model is not capable of predicting the depo-

sition uniformity. Nonetheless useful insight can be gained on the effect of pulse period and duty cycle on the deposition rate. The main advantage of the CSTR model is that an analytic solution can be readily obtained assuming linear reaction kinetics. Even for nonlinear kinetics, a solution to the CSTR model can be obtained much faster than for the axial dispersion model. Furthermore, the linear CSTR solution may be used as a building block for obtaining an analytic solution to the linear time-dependent dispersion model, since the dispersion reactor can be modeled as a cascade of CSTRs.

For the purpose of the CSTR model, a simplified reaction scheme was assumed as shown below, i.e., volume recombination of the radicals was neglected



The dimensionless concentration of the radicals C_1 and of the precursor gas C_2 (normalized with respect to the total gas concentration) were found by solving the equations

$$\frac{dC_1}{dT} = -(k_s\tau + 1)C_1 + k_p(T)\tau C_2 \quad [B-1]$$

$$\frac{dC_2}{dT} = C_{2F} - (k_p(T)\tau + 1)C_2 \quad [B-2]$$

where $\tau = V/Q$ is the gas residence time, $k_s = k_n(S/V)_n$ is the rate constant of the surface reaction, $(S/V)_n$ is the surface-to-volume ratio, V is the reactor (plasma) volume, and Q is the gas flow rate under the reactor conditions. $C_{1F} = 0$ and C_{2F} are the feed concentrations of the radical and the precursor gas, respectively.

Equations [B-1] and [B-2] were solved for the periodic steady state by requiring that the species concentrations are identical at the start and end of a cycle. For example, for the j^{th} cycle $jT_p \leq T < (j+1)T_p$, one requires $C_i(jT_p) = C_i((j+1)T_p)$. By defining $\theta = (T - jT_p)/T_p$ and f_d as the plasma-on fraction of the period (duty cycle), the solution for the precursor gas concentration can be written as

for $0 \leq \theta < f_d$

$$C_2(\theta) = \frac{C_{2F}}{(k_p\tau + 1)} + \left[C_{2i} - \frac{C_{2F}}{(k_p\tau + 1)} \right] \exp\left(- (k_p\tau + 1) \frac{\tau_p}{\tau} \theta\right)$$

for $f_d \leq \theta < 1$

$$C_2(\theta) = C_{2D} \exp\left(-\frac{\tau_p}{\tau}(\theta - f_d)\right) + C_{2F} \left[1 - \exp\left(-\frac{\tau_p}{\tau}(\theta - f_d)\right) \right]$$

$$C_{2,av} = \frac{C_{2F}f_d}{(k_p\tau + 1)} + \left[C_{2i} - \frac{C_{2F}}{(k_p\tau + 1)} \right] \frac{\left(1 - \exp\left(- (k_p\tau + 1) \frac{\tau_p}{\tau} f_d\right)\right)}{(k_p\tau + 1) \left(\frac{\tau_p}{\tau}\right)} + C_{2F}(1 - f_d) + \frac{(C_{2D} - C_{2F})}{\left(\frac{\tau_p}{\tau}\right)} \left(1 - \exp\left(-\frac{\tau_p}{\tau}(1 - f_d)\right)\right)$$

where $C_{2,av}$ is the time-average precursor gas concentration, and

$$C_{2i} = \frac{C_{2F} \left[1 - \exp\left(-\frac{\tau_p}{\tau}(1 - f_d)\right) \right] + \frac{C_{2F}}{(k_p\tau + 1)} \left[\exp\left(-\frac{\tau_p}{\tau}(1 - f_d)\right) - \exp\left(- (k_p\tau f_d + 1) \frac{\tau_p}{\tau}\right) \right]}{\left(1 - \exp\left(- (k_p\tau f_d + 1) \frac{\tau_p}{\tau}\right)\right)}$$

$$C_{2D} = \frac{C_{2F}}{(k_p\tau + 1)} + \left(C_{2i} - \frac{C_{2F}}{(k_p\tau + 1)} \right) \exp \left(- (k_p\tau + 1) \frac{\tau_p}{\tau} f_d \right)$$

The solution for the radical concentration is (assuming $k_p \neq k_s$)

for $0 \leq \theta < f_d$

$$C_1(\theta) = (C_{1i} - \alpha) \exp \left(- (k_s\tau + 1) \frac{\tau_p}{\tau} \theta \right) + k_p\tau \left[\frac{C_{2F}}{(k_s\tau + 1)(k_p\tau + 1)} + \frac{C_{2i} \exp \left(- (k_p\tau + 1) \frac{\tau_p}{\tau} \theta \right)}{(k_s\tau - k_p\tau)} - \frac{C_{2F} \exp \left(- (k_p\tau + 1) \frac{\tau_p}{\tau} \theta \right)}{(k_p\tau + 1)(k_s\tau - k_p\tau)} \right]$$

for $f_d \leq \theta < 1$

$$C_1(\theta) = C_{1D} \exp \left(- (k_s\tau + 1) \frac{\tau_p}{\tau} (\theta - f_d) \right)$$

The time-average radical concentration is given by

$$C_{1,av} = \frac{(C_{1i} - \alpha)}{(k_s\tau + 1) \frac{\tau_p}{\tau}} (1 - \exp \left(- (k_s\tau + 1) \frac{\tau_p}{\tau} f_d \right)) + k_p\tau \left[\frac{C_{2i}}{(k_s\tau - k_p\tau)(k_p\tau + 1) \frac{\tau_p}{\tau}} - \frac{C_{2F}}{(k_p\tau + 1)^2(k_s\tau - k_p\tau) \frac{\tau_p}{\tau}} \right] \left(1 - \exp \left(- (k_p\tau + 1) \frac{\tau_p}{\tau} f_d \right) \right) + \frac{k_p\tau C_{2F} f_d}{(k_p\tau + 1)(k_s\tau + 1)} \left(1 - \exp \left(- (k_s\tau + 1)(1 - f_d) \frac{\tau_p}{\tau} \right) \right) + C_{1D} \frac{(1 - \exp \left(- (k_s\tau + 1)(1 - f_d) \frac{\tau_p}{\tau} \right))}{(k_s\tau + 1) \frac{\tau_p}{\tau}}$$

where

$$\alpha = k_p\tau \left[\frac{C_{2i}(k_s\tau + 1) - C_{2F}}{(k_s\tau + 1)(k_s\tau - k_p\tau)} \right]$$

$$\beta = k_p\tau \left[\left(\frac{C_{2i}}{(k_s\tau - k_p\tau)} - \frac{C_{2F}}{(k_p\tau + 1)(k_s\tau - k_p\tau)} \right) \exp \left(- (k_p\tau + 1) \frac{\tau_p}{\tau} f_d \right) + \frac{C_{2F}}{(k_p\tau + 1)(k_s\tau + 1)} \right]$$

$$C_{1i} = \frac{\left(\beta \exp \left((k_s\tau + 1) \frac{\tau_p}{\tau} f_d \right) - \alpha \right) \exp \left(- (k_s\tau + 1) \frac{\tau_p}{\tau} \right)}{1 - \exp \left(- (k_s\tau + 1) \frac{\tau_p}{\tau} \right)}$$

$$C_{1D} = (C_{1i} - \alpha) \exp \left(- (k_s\tau + 1) \frac{\tau_p}{\tau} f_d \right) + \beta$$

The utility of the CSTR model is demonstrated by two examples below. For instance, at the limit of long pulse periods $\tau_p/\tau \gg 1$ (and for $f_d \neq 0$) the equation for $C_{1,av}$ above yields

$$C_{1,av} = \frac{k_p\tau C_{2F} f_d}{(k_p\tau + 1)(k_s\tau + 1)}$$

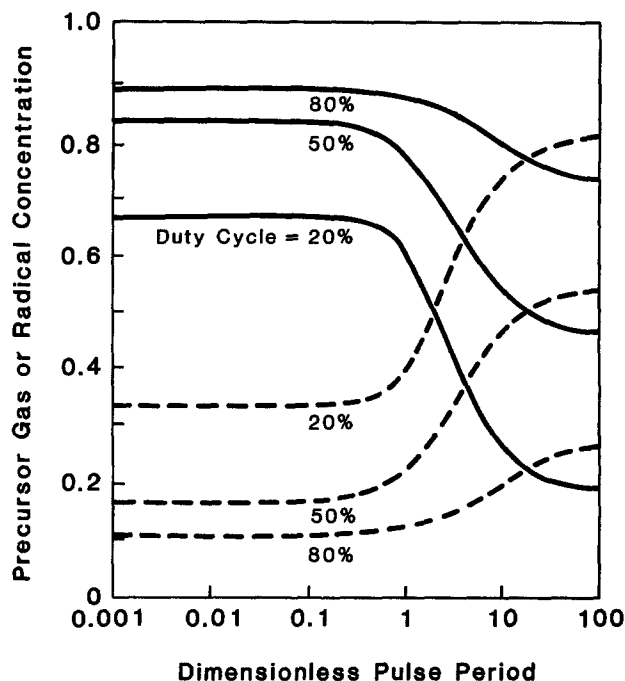


Fig. B-1. Dimensionless precursor gas concentration (dashed line) and radical concentration (solid line) in a well-mixed pulsed-plasma reactor as a function of the dimensionless pulse period, $k_p\tau = 10$, $k_s\tau = 1$.

One notes that, under such condition, the average radical concentration (and reaction rate) is equal to the CW concentration multiplied by the duty cycle. As a second example, consider the effect of pulse period and duty cycle on deposition rate. Figure B-1 demonstrates such effect for $k_p\tau = 10$ and $k_s\tau = 1$. The radical concentration (proportional to deposition rate) and the precursor gas concentration are shown as a function of the dimensionless pulse period τ_p/τ with the duty cycle f_d as a parameter. By comparing to Fig. 9, one observes that the CSTR model captures the mean features of the process. However the CSTR model cannot predict the deposition uniformity. The CSTR model may be a good approximation of the dispersion model when the species diffusivity is very high ($Pe \rightarrow 0$). Under such condition, the deposition profiles are expected to be spatially uniform.

LIST OF SYMBOLS

- a_{ij} coefficients, Eq. [25]
- B_j^{kn} B-spline of order k (and $n - 1$ continuity) at point j , Eq. [25]
- c total gas concentration, mols/cm³
- c_i concentration of species i , mols/cm³
- c_{iF} feed concentration of species i , mols/cm³
- C_i dimensionless concentration of species i
- C_1 dimensionless concentration of radicals
- C_p dimensionless concentration of precursor gas
- C_{iF} dimensionless feed concentration of species i
- D_i diffusivity of species i , cm²/s
- D_1 diffusivity of radicals, cm²/s
- Da_p Damkohler number of radical production, Eq. [10]
- Da_n Damkohler number for radical deposition, Eq. [10]
- Da_v Damkohler number for volume recombination, Eq. [10]
- f_d duty cycle
- G_i net generation rate of species i , mols/cm³-s
- k_p rate constant for radical production, cm³/s
- k_n rate constant for radical deposition, cm/s
- k_v rate constant for radical volume recombination, cm⁶/mol²-s
- L reactor length, cm
- N_b number of collocation points, Eq. [25]-[27]
- N_p number of pulses (cycles)
- n_e electron density, 1/cm³
- p pressure, dynes/cm² or torr
- Pe Peclet number, Eq. [11]
- R recycle ratio
- R_g universal gas constant, 62,358 torr-cm³/mol-K
- R_t tube radius, cm

τ	dimensionless deposition rate
$(S/V)_n$	surface to volume ratio, cm^{-1}
T	dimensionless time, Eq. [9]
T_g	gas temperature, K
T_1	power-on fraction of pulse period
T_2	power-off fraction of pulse period
T_p	dimensionless pulse period, Eq. [9]
t	time, s
u	linear gas velocity, cm/s
UI	uniformity index, Eq. [21]
x	axial coordinate, cm

Greek

ϵ_{PSS}	error tolerance for detection of periodic steady state, Eq. [30]
θ	time as a fraction of the pulse period during a single period
Λ	radical diffusion length, cm
ξ	dimensionless axial coordinate, Eq. [9]
ξ_j	set of collocation points, Eq. [26]
τ	gas residence time, Eq. [9]
τ_p	pulse period, s

REFERENCES

- D. M. Manos and D. L. Flamm, "Plasma Etching: An Introduction," Academic Press, New York (1989).
- B. Chapman, "Glow Discharge Processes," John Wiley, New York (1980).
- A. R. Reinberg, *J. Electron. Mater.*, **8**, 345 (1979).
- A. Sherman, "Chemical Vapor Deposition for Microelectronics," Noyes Publications, Park Ridge (1987).
- M. J. Kushner, *J. Appl. Phys.*, **63**, 2532 (1988).
- R. J. Jensen, A. T. Bell, and D. S. Soong, *Plasma Chem. Plasma Process.*, **3**, 139 (1983).
- C.-P. Chang, D. L. Flamm, D. E. Ibbotson, and J. A. Mucha, *J. Appl. Phys.*, **63**, 1744 (1988).
- G. Turban and Y. Catherine, *Thin Solid Films*, **48**, 57 (1978).
- G. Turban, Y. Catherine, and B. Grolleau, *ibid.*, **60**, 147 (1979).
- I. Chen, *ibid.*, **101**, 41 (1983).
- L. E. Kline, W. D. Partlow, and W. E. Bies, *J. Appl. Phys.*, **65**, 70 (1989).
- R. S. Rosler and G. M. Engle, *Solid State Technol.*, p. 172, April 1981.
- H. Y. Kumagai, in "Chemical Vapor Deposition 1984," McD. Robinson, G. W. Cullen, C. H. J. van den Brekel, J. M. Blocher, Jr., and P. Rai-Choudhury, Editors, p. 189, The Electrochemical Society Soft-bound Proceedings Series, PV 84-6, Pennington, NJ (1984).
- L. J. Overzet, J. T. Verdeyen, R. M. Roth, and F. F. Carasco, *Mater. Res. Soc. Symp. Proc.*, **98**, 321 (1987).
- Y. Watanabe, M. Shiratani, Y. Kubo, I. Ogawa, and S. Ogi, *Appl. Phys. Lett.*, **53**, 1263 (1988).
- R. W. Boswell and R. K. Porteous, *J. Appl. Phys.*, **62**, 3123 (1987).
- S. G. Hansen, G. Luckman, and S. D. Colson, *Appl. Phys. Lett.*, **53**, 1588 (1988).
- S.-K. Park and D. J. Economou, *This Journal*, Submitted.
- G. I. Taylor, *Proc. R. Soc. London, Ser. A*, **219**, 186 (1953).
- W. R. Schmeal and N. R. Amundson, *AIChE J.*, **12**, 1202 (1966).
- L. Lapidus and W. E. Schiesser, "Numerical Methods for Differential Systems," Academic Press, New York (1976).
- B. A. Finlayson, "Nonlinear Analysis in Chemical Engineering," McGraw-Hill, New York (1980).
- A. C. Hindmarch, in "Advances in Computer Methods for Partial Differential Equations • IV," R. Vichnevetsky and R. S. Stepleman, Editors, p. 312, IMACS, North Holland Publishing Co. (1981).
- A. C. Hindmarch, in "Scientific Computing," R. Stepleman *et al.*, Editors, p. 55, IMACS, North-Holland Publishing Co. (1983).
- A. C. Hindmarch, *ACM-SIGNUM Newsletter*, **15** (4), 10 (1980).
- C. DeBoor, *SIAM J. Numer. Anal.*, **14**, 441 (1977).
- D. Ramkrishna and N. R. Amundson, "Linear Operator Methods in Chemical Engineering with Applications to Transport and Chemical Reaction Systems," Prentice-Hall Inc., Englewood Cliffs, NJ (1985).
- S.-K. Park and D. J. Economou, *J. Appl. Phys.*, **66**, 3256 (1989).
- C. Ozgen and Z. Hicsasmaz, *Chem. Eng. Sci.*, **42**, 1413 (1987).
- A. H. Wan and H. Y. Cheh, *This Journal*, **135**, 643 (1988).
- H. B. Keller, in "Mathematical Aspects of Chemical and Biochemical Problems and Quantum Chemistry," D. S. Cohen, Editor, p. 85, American Mathematical Society, Providence, RI (1974).
- K. F. Jensen and D. B. Graves, *This Journal*, **130**, 1951 (1983).

Mathematical Modeling of an H₂S Removal Electrolyzer

Z. Mao,* P. Adanuvor,** and R. E. White**

Department of Chemical Engineering, Texas A&M University, College Station, Texas 77843

ABSTRACT

A mathematical model is presented for a high temperature H₂S electrolyzer. It is shown that the maximum current in this type of a cell is determined entirely by the transport rate of sulfide ions through the separator. It is suggested that this model could be used to determine the feasibility of various designs for this electrolyzer.

It has long been recognized that electrolysis of hydrogen sulfide (H₂S) would provide an effective means of cleaning various H₂S containing gases (1-3); consequently, a great deal of effort has been devoted to develop such a process. Unfortunately, electrolysis of H₂S in aqueous solutions leads to problems such as the passivation of the anode because of the deposition of sulfur (4), and the oxidation of sulfide or sulfur into sulfur oxyanions (5). The application of high temperature molten salts for this electrolysis may provide a means to overcome these problems because sulfur would be in a liquid or even a gaseous state at high temperatures, which would remove the "blocking" effect caused by elemental sulfur in the aqueous process. Also, because no oxygen would be present in the salts, neither sulfide nor other sulfur species would be oxidized into sul-

fur oxyanions. Several attempts have been made recently to use an electrolyzer similar to the molten carbonate fuel cell for this purpose (3, 6-8). While these experiments were carried out without much success, high polarization losses were experienced, the results of these experiments emphasized that improvement in the performance of these cells may be obtained by optimizing the cell design in a manner analogous to that for the molten carbonate fuel cell. Little attention has been paid to differences between these two types of electrochemical reactors. This work uses a mathematical model to examine the characteristics of the electrolyzer with regard to mass transport and to predict the maximum current density that could be obtained with this type of an electrolyzer.

Although the structure of the electrolyzer is similar to that of the molten carbonate fuel cell, the mass transport process is different from that of the molten carbonate fuel cell (MCFC). In the latter, the reactants are fed to both elec-

* Electrochemical Society Student Member.

** Electrochemical Society Active Member.